Available free online at www.medjchem.com

Mediterranean Journal of Chemistry

Mediterranean Journal of Chemistry **2019**, 9(3), 236-248

Calcite, the main corrosion inhibitor contained in the raw clay (Rhassoul) of brass in 3% NaCl medium

Nordin Ben Seddik [1,*], Ihssane Raissouni [1], Khalid Draoui [1], Ahmed Aït Aghzzaf [2], Anas Chraka [1], Badr Aznag [3], Faiza Chaouket [1] and Dounia Bouchta [1]

[1] Materials and interfacial systems, Laboratory, ERESI team, Faculty of Sciences, Department of Chemistry, Tetouan, 93002, Morocco

[2] Laboratoire des Sciences Appliquées et Didactique (LaSAD), École Normale Supérieure, Tetouan, Maroc

[3] Research Center, REMINEX-Groupe, MANAGEM, Hajar site, BP 469, Marrakech, Morocco

Abstract: Corrosion control of copper alloys such as brass is of great interest to researchers and scientists. Clays become materials of choice as corrosion inhibitors and as their reservoir in corrosive environments. The effect of Rhassoul on the corrosion of Cu-36Zn alloy in 3% NaCl solution has been studied. Electrochemical techniques showed that the optimum concentration was 1g/L showing the highest inhibition efficiency (82%). This concentration was evaluated at five different temperatures. In order to determine the influence of purification, this result was compared to that of the homoionic clay labeled Na^+-ST and to the pure calcite. Chemical composition of the brass specimen and solutions were done by inductively coupled plasma atomic emission spectrometry (ICP-AES) and atomic absorption (AA) respectively. The effectiveness of this clay against the dissolution of Zinc reached 61%. XRD technique demonstrated the homoionization of this clay by shifting the basal spacing d_{001}.

Keywords: Rhassoul; Corrosion; Stevensite; Basal spacing; Brass.

1. Introduction

Corrosion is the deterioration of a metal by an aggressive agent or a chemical reaction with its environment. It is a permanent problem, difficult to eliminate. Corrosion affects most industrial sectors and can cost billions of dollars each year [1]. As an alternative to steel, Brass is used in different domains thanks to its excellent processability, aesthetic appearance, ease of production and high resistance [2]. This alloy is likely to corrode under certain circumstances, especially in a chloride-containing aqueous medium such as seawater which contains a significant concentration of dissolved salts and is very corrosive. Many efforts are being made to limit corrosion in marine environments, as industries develop and implement solutions to prevent degradation of these materials. Several methods were used to reduce the high economical cost by protecting this relatively noble metal from corrosion, and among which, are corrosion inhibitors: benzotriazole and its derivatives have been used by several authors [3-7]. Chromate was used for a long time [8,9]. These compounds have shown better corrosion inhibition but may damage the environment due to its toxicity. In terms of protection of the environment, essential oils were tested, where *eugenol* [10] and *Ammi visnaga (L.) Lam* [11], were the inhibitors. Results showed high inhibition performances of brass in 3% NaCl solution. Thanks to their many advantages, clays were recently studied [12,13]. Halloysite, as a biocompatible nano-container material [14], has been used to encapsulate benzotriazole and incorporated it into a coating matrix.

Aït Aghzzaf et al., [15] studied the effects of modified beidellite mineral clay by calcium ions on the inhibition of Zinc from corrosion in NaCl medium, this inhibitor was precipitated in the form of calcite in the presence of carbonate ions. The same author investigated the effect of grafted palygorskite for corrosion protection of steel by heptanoic acid in chloride medium [16,17]. The corrosion mechanism of brass in the chloride-containing medium was described According to a recently published article [18] as follows: the brass surface upon reaching the potential corrosion E_{corr} in the anodic area is passivated resulting in the formation of oxide/hydroxide of the brass film. This later rapidly deteriorated when potential

*Corresponding author: Nordin Ben Seddik
E mail: n.benseddik@uae.ac.ma
DOI: http://dx.doi.org/10.13171/mjc93191016530nbs

Received July 9, 2019
Accepted September 17, 2019
Published October 16, 2019

increased leading to chloro-complexes of Cu(I), Cu(II) and Zn(II). The objective of our study is to simplify the manipulation of a new alternative compound to fight against corrosion of brass in 3% NaCl solution. An abundantly, safety and green raw clay was used without pretreatment. "Rhassoul" as described by several authors. It is a magnesian smectite [19-21] with a high rate of Stevensite clay fraction. In order to assess the effectiveness of these new alternative inhibitors and understand how this inhibition occurs. Various concentrations of Rhassoul were immersed in 3% NaCl solution in contact with a brass surface, followed by a study on the effect of temperature. The corrosion protection brought by the optimum concentration of this raw clay was compared to the same concentration of the homoionic one labeled Na^+-ST and to the equivalent concentration of pure calcite $CaCO_3$ at 298°C. In these conditions, in order to predict the synergistic feasibility of the calcite and the purified clay fraction in the raw Rhassoul, the electrochemical behavior of brass was monitored by electrochemical techniques such as potentiodynamic curves, and electrochemical impedance spectroscopy (EIS). While the surface morphological study was carried out using scanning electron microscopy (SEM) and the composition of the brass surface was analyzed using energy dispersive X-ray analysis (EDS). The concentrations of dissolved copper and zinc in the electrolyte were calculated using atomic absorption technique. X-ray diffraction and ICP-AES techniques were used to characterize raw and purified Rhassoul.

2. Experimental

2.1. Raw clay (Rhassoul)

The studied clay is located in Jebel Rhassoul in the mountains of the Atlas of Morocco. This clay presents a high rate of Stevensite fraction. It is recovered and dried at 100°C to remove water, then crushed and sieved. Only aggregates with a diameter of 20 μm (micrometer) were selected. Chemical composition (expressed in weight percent wt. %) of raw Rhassoul is: Si: 19.78, Mg: 10.76, Ca: 7.65, Al: 1.32, Fe: 0.92, Sr: 0.17, Ti: 0.13, Na: 0.08. The concentration ranges of raw and purified clay used for this study were 0.5, 0.8 and 1g/L.

2.2. NaCl aqueous solution and Calcite powder

NaCl and Calcite powders were purchased from Scharlab S.L to prepare the aqueous solution at (3% wt.) simulated to the seawater for the first and to confirm the responsibility of corrosion protection for the second.

2.3. Metal electrode

The working electrode used for the electrochemistry tests is in brass having the chemical composition of 64% Cu, 36% Zn, 0.0151% Fe, 0.0012% Ni, 0.0033% Pb, 0.0016% Se and 0.0019% Sn, expressed in weight percent. The brass plates are cut into discs of 1cm in diameter and mechanically polished with abrasive papers of different grades (from 600 to 1200).

2.4. Clay treatment

Raw Rhassoul has undergone purification treatments to eliminate the accessory minerals (quartz, dolomite, carbonates ...). The purification procedure was as follows:

The raw clay sample was firstly ground and sieved in order to obtain excellent powders at 20 μm in order to reduce the number of impurities by eliminating the corresponding large particles which consequently facilitates further purification operations.

Secondly, decarbonisation to remove all carbonate phases (dolomite and calcite) that may exist, by attacking the samples with hydrochloric acid solution 1M. For that reason, 30 grams of the obtained powder are dispersed in bidistilled water in a 1L flask with stirring for 30 min (minute). Then a solution of 1M HCl is added gradually (whose action on the decomposition of carbonates is accompanied by the release of CO_2 bubbles) until the effervescence stops and the stirring is continued for 1 hour. Note that in order not to destroy the clay fraction of Stevensite, we opted firstly for the use of an acetic acid/sodium acetate buffer solution which has the advantage of setting the pH at a suitable value (4.5 in our case) throughout the process.

The Stevensite dispersion obtained is homoionized by exchange reaction of the charge compensator ions (Ca^{2+}, Mg^{2+} and K^+) by the Na^+ cations. This operation was carried out by dispersing the clay in a solution of sodium chloride (NaCl) 1mol.L^{-1} for 24 hours with stirring. The clay fractions, flocculating in the presence of salt, were easily recovered, washed several times with bidistilled water and then centrifuged several times at 4000 round per minute (rpm) for 5 min. Obtaining a stable dispersion is favored by the almost total elimination of the chloride ions evidenced by the $AgNO_3$ test. Na^+-ST, having a particle size less than 2 µm in diameter [22], was isolated from this clay when transferring this stable dispersion to a 2L test tube and adding the bidistilled water up to the gauge line. After a giving time (t (min)) the size of our particles (d (µm)) were sedimented to a known depth from the mark (x (cm)). This process is governed by Stokes's law [23] equation Eq. 1.

$$t = \frac{190X}{d^2} \quad (1)$$

After 24 hours, our fine fraction (d=2 µm) is taken for a depth of about x=30 cm and completed with the bidistilled water to the previous mark. This operation is repeated until the dispersion is almost transparent.

Our collected dispersion is then centrifuged at 4000 rpm for 40 min to recover the Stevensite clay fractions. This later is dried at 60 °C, crushed and then stored under laboratory conditions.

2.5. Instrumentation

Experimental measurements were carried out using a potentiostat/galvanostat PGZ301, equipped with voltamaster software, accompanied by a double-walled pyrex glass cell to check the homogeneity of the solution. In this cylindrical cell were immersed three electrodes which are the working electrode WE (brass) masked with polyester and having an active surface area of 0.785 cm^2 (square centimeter), the reference electrode RE with saturated calomel (SCE) (E_{SCE} = 0.241 V (volt)) and a platinum counter-electrode CE to ensures the flow of electric current in the working electrode through the solution. Before running each experiment, the surface of the working electrode was polished mechanically by using emery paper of 600, 800, 1000 and 1200 grades, washed with bidistilled water and then dried. During the experiments, the solution was stirred with a magnetic stirrer at a constant speed. During all measurements, solutions were exposed to the atmosphere in a controlled temperature using a thermostat. Those measurements were done after 1 h immersion time with stirring and were repeated at least three times in order to obtain the same result.

The potentiodynamic current/potential curves in 3% NaCl solution were obtained by automatically changing the electrode potential from -0.7 to +0.2 V (V/SCE), at a scanning- rate of 0.5 mV/s (millivolt per second).

Nyquist and bode (module and phase) plots were obtained from EIS experiments at open circuit potential (OCP) after 1 hour of immersion in the corrosive solution. The measured frequency range was from 100 kHz (Kilohertz) to 10 Mhz (millihertz) with disturbance amplitude of 10 mV at the corrosion potential with 10 points per decade. To interpret the results of impedance spectroscopy, electrochemical interfaces (electrode/electrolyte) were modeled by equivalent electrical circuits using EC-LAB V10.40 software.

2.6. Surface morphology and composition

After polarization experiments in corrosive medium, washing with distilled water and drying carefully, the brass specimens surface was visualized by a SUTW-Sapphire, Resolution: 131.40, Lsec: 10 Scanning Electron Microscope (SEM) connected to an energy dispersive X-ray analyzer (EDS) using SH-4000M model.

Concentrations of Zn^{2+} and Cu^{2+} in the electrolytes, after polarization experiments in the presence and absence of 1g/L of raw clay and were determined by atomic absorption technique using Varian Spectra AA 220 FS. This technique was used to measure the amount of dissolved zinc and copper from the brass surface. The chemical compositions (wt. %) of the brass and raw clay samples were determined by Inductively Coupled Plasma atomic emission spectrometry (ICP-AES) technique using ULTIMA 2CE.

3. Results and Discussion

3.1. Chemical characterization of raw Rhassoul and Na^+-ST

Rhassoul is a mixture of clay fractions whose Stevensite presents the majority [24] (84.2 wt %). In **Fig. 1**(a), the XRD pattern of natural Rhassoul shows that the dominant phase is the Stevensite, whose characteristic peaks [25] at 2θ = 5.74°, 2θ = 12.46°…, and from the International Centre for Diffraction Data (ICDD), we note the presence of quartz (ICDD: 03-065-0466), dolomite (ICDD: 01-083-1766) and calcite (ICDD: 01-072-4582). 2θ refers to the angle of reflection.

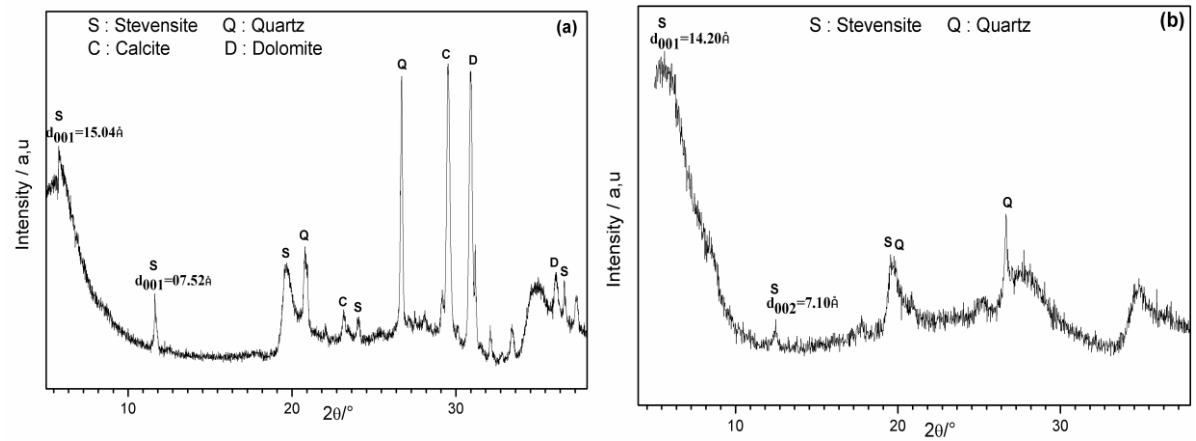

Figure 1. XRD patterns of (a) raw Rhassoul and (b) Na^+-ST

In the purified clay (Fig. 1(b)), we can notice the presence of Stevensite phase and the absence of calcite and other impurities provided by the diffractogram. The XRD pattern of raw Rhassoul sample in Fig. 1(a), reveals a well resolved (001) reflection centred at a basal spacing d_{001} = 15.04 Å (angstrom), corresponding to cations such as Na^+, Mg^{2+} and K^+, Upon ion exchange with sodium cations illustrated in Fig. 2. The Stevensite basal spacing shifts to about 14.20 Å (Fig. 1(b)), which is indicative of the saturation of Stevensite interlayer spaces with Na^+ ions surrounded with equivalent layers of water molecules [26,23]. Note that the Stevensite as a magnesian pole of the smectite series constitutes the majority phase of this raw clay with the presence of free silica and quartz in small quantities. The 2θ peaks at 25.27° and 48.01° confirm the anatase structure of TiO_2. The broad diffraction peaks indicate small size crystallite [27]. These results are in good agreement with the chemical composition of this purified clay shown in Table 1.

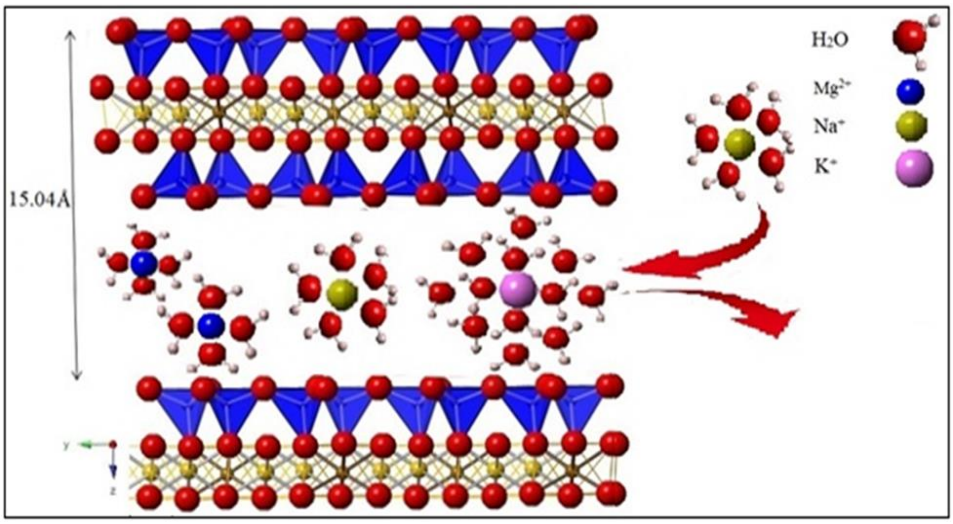

Figure 2. Scheme showing the exchange mechanism between Na^+ and interlayer cations present in the natural Stevensite.

Table 1. Mass Percentage obtained from ICP-AES technique of different elements composing Na^+-ST.

	SiO_2	Al_2O_3	Fe_2O_3	CaO	MgO	K_2O	MnO	TiO_2	P_2O_5	Na
Na^+-ST %	57.15	3.50	1.82	<0.10	26.91	1.11	<0.01	0.22	0.05	1.63

3.2. Electrochemical study

Fig. 3 presents the potentiodynamic polarization curves for brass in absence and presence of different concentrations of raw Rhassoul, obtained from an aerated 3% NaCl solution after one-hour immersion time. For all concentrations, the cathodic curves present a diffusion plateau. This plateau was attributed to the reduction of dissolved oxygen [28], following the reaction given in Eq. 2.

$$O_2 + 2H_2O + 4e^- \rightarrow 4OH^- \qquad (2)$$

The cathodic current density of the brass was significantly reduced after adding different concentrations of raw Rhassoul, and no significant change was detected in the shape of the cathodic curves, it can be said that the cathodic process remained the same, indicating the precipitation of clay components on the brass surface [29], thus the delay of corrosion without altering the cathodic reaction mechanism by blocking the active sites [30,31]. This suggests that the investigated raw Rhassoul is a cathodic type inhibitor. Mixed process of diffusion and activation was observed at the corrosion potential [32]. The same author [32] indicates that when studying the electrochemical behavior of copper in neutral aerated medium, the presence of a reduction peak in the cathodic area is in agreement with the reduction peak attributed to the reduction of Cu_2O formed by the hydrolysis of the primary cuprous corrosion products. The anodic process was not affected by the addition of raw clay. According to Avramovic and Antonijevic [33], the presence of anode peaks on the anodic polarization curves is due to an active dissolution of the samples and formation of Cu(I)-chloro-complex ($CuCl_2^-$) formed by a primary reaction Eq. 3.

$$Cu + 2Cl^- \rightarrow CuCl_2^- + 1e^- \qquad (3)$$

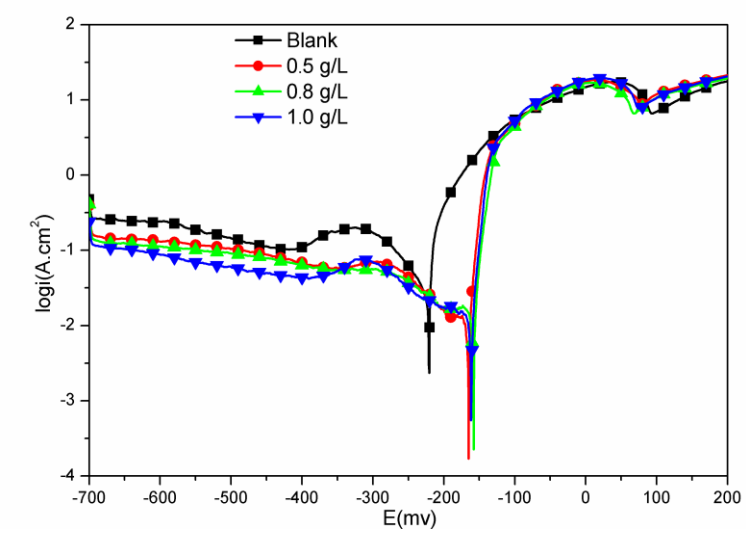

Figure 3. Polarization curves of the studied raw clay in 3% NaCl solution.

When increasing potential, the anodic current density decreases and a passive film of zinc oxide/hydroxide was formed. Rapidly this later deteriorates and a Zn(II)-chloro-complex is released in the electrolyte. Table 2 presents the corrosion current density (I_{corr}), corrosion potential (E_{corr}) and cathodic slopes (βc) (millivolt per decade). The inhibition efficiency (I_E (%)) was calculated using the following Eq. 4. Where I_{corr} and $I_{corr}(inh)$ correspond to the current densities in the absence and presence of raw Rhassoul, respectively.

Table 2. Polarization parameters of brass in the absence and presence of different concentrations of the raw clay.

Concentration (g/L)	**-E_{corr} (mV/SCE)**	**I_{corr} (µA/cm²)**	**-β_c (mV/dec)**	**Inhibition efficiency I_E (%)**
Blank	220	73.0	307	-
0.5	156	19.5	200	73.5
0.8	154	19.0	197	74.0
1	151	13.0	161	82.3

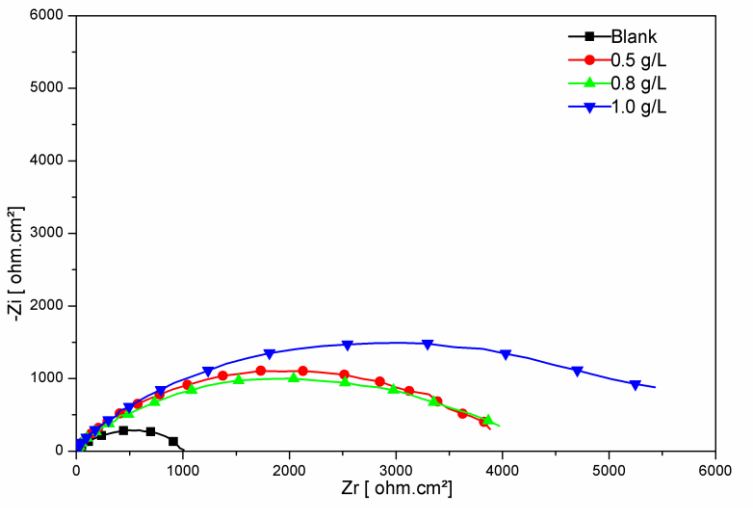

Figure 4. Nyquist plot of brass in 3% NaCl solution at different concentrations of raw Rhassoul at 298°K.

$$I_E(\%) = \frac{I_{corr} - I_{corr}(inh)}{I_{corr}} \times 100 \qquad (4)$$

The inhibition efficiency values increase, and those of corrosion current densities decrease with the increasing concentrations, reaching 82.3% and 13.0µA/cm² (microampere per square centimeter), respectively. This might be possible proof that the raw clay or some of its components

precipitate on the brass surface, preventing it from corrosion.

Fig. 4 shows the Nyquist plot of the brass at different concentrations measured at the corrosion potential, without and with the three inhibitor concentrations. The diagram shows a depressed semicircle throughout

the measured frequency range, this shape is probably caused by the heterogeneity of the surface. The diameter of the semicircle increases simultaneously by increasing concentrations.

Taking into account the low chi-squared value, experimental Nyquist data were fitted to an equivalent circuit with and without raw clay (Fig. 5). The constant phase element (CPE) was used to consider the non-ideality of the system being investigated (as will be indicated from SEM observations) and represented by Eq. 5.

$$Z_{CPE} = [Q \times (j\omega)^n]^{-1} \qquad (5)$$

Where: (n) is the CPE exponent attributed to deviation from ideal capacitive behavior, (ω) the angular frequency and (j) for the imaginary unit. R_e, R_{ct}, CPE_1, R_f and CPE_2 are electrolyte resistance, charge transfer resistance, capacitance related to the double layer, film resistance formed on the surface and the corresponding capacitance, respectively. The film resistance is attributed to the weak corrosion products layer in the new solution. When using the inhibitor, this layer is reinforced by a compact one due to the precipitation of the element responsible for the inhibition in addition to some corrosion products.

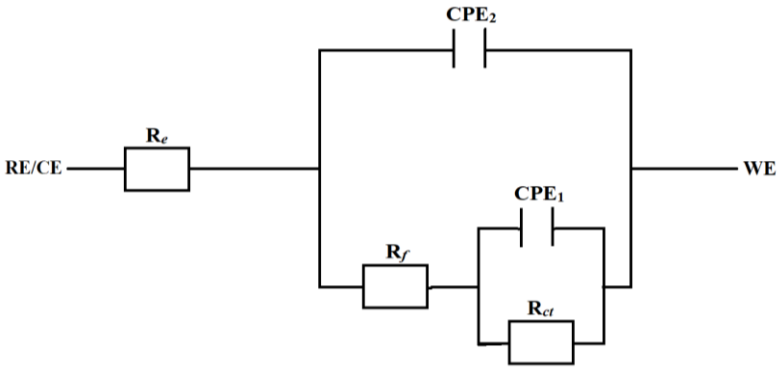

Figure 5. Equivalent electrical circuit used for computer fitting of the experimental data for the brass surface in the absence and presence of different concentrations of raw clay

The extrapolation to 10 Mhz frequency in the bode-magnitude plot (Fig. 6(b)), permits to get the polarization resistance R_p and consequently calculate the inhibition percentage E' which is defined by the following Eq. 6. Where Rp and Rp(inh) denote the polarization resistances without and with inhibitor, respectively.

$$E' = \frac{R_P(inh) - R_p}{R_p} \times 100 \qquad (6)$$

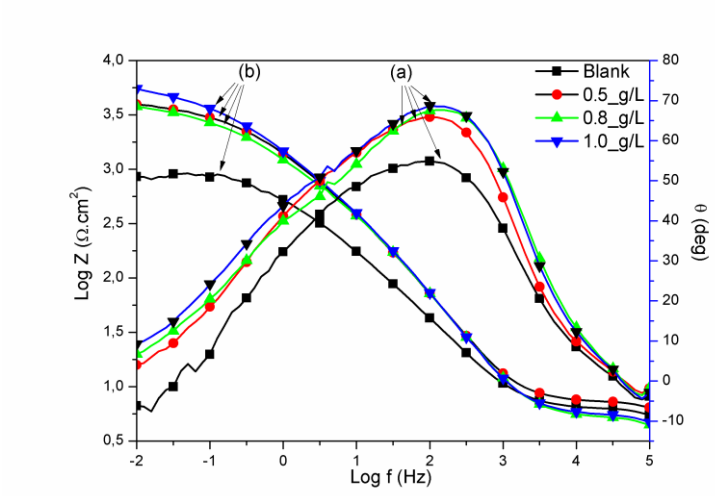

Figure 6. Electrochemical impedance: (a) Bode phase and (b) Bode module of brass in 3% NaCl solution at different concentrations of raw Rhassoul at 298°K

Bode-phase plot (Fig. 6(a)) shows two-time constants related to the charge transfer resistance R_{ct} and the low corrosion products resistance R_f (without inhibitor). When adding the raw clay, the

second time constant appeared in low frequency, which refers to the precipitated film resistance R_f in parallel with the corresponding capacitance CPE_2. Polarization resistance R_p and inhibition efficiency E' (%) values were mentioned in Table 3.

Table 3. Rp and E' values of brass immersed in 3% NaCl medium in the absence and presence of different concentrations of raw Rhassoul.

	Blank	**0.5 g/L**	**0.8 g/L**	**1 g/L**
Rp(Ω.cm²)	1088	4080	4150	6030
E' (%)	-	73.3	73.7	82.0

Table 4 indicates that; all resistances increase when increasing the concentration of raw clay. Furthermore, CPE_1 and CPE_2 values tend to decrease and the inhibition efficiency increases (where F and S denote Farad and Siemens, respectively), lets conclude that from one hand there is an increase in the thickness of the electrical double layer and that corrosion product are less susceptible to the redox process, from the other hand there is increase of real surface area which is partly due to the formation of the corrosion products and also to the precipitation of the clay fraction and/or some of the raw clay components on the metal/solution interface [7].

Table 4. Parameters of the equivalent circuit elements calculated from the fitting results of EIS data at different concentrations.

Concentration (g/L)	**R_e (Ohm)**	**$CPE_1\times10^{-6}$ ($F.s^{(n-1)}$)**	**R_{ct} (Ohm)**	**n_1**	**$CPE_2\times10^{-6}$ ($F.s^{(n-1)}$)**	**R_f (Ohm)**	**n_2**
Blank	5.3	391	1081	1.00	035	010	0.59
0.5	5.5	057	3709	0.87	234	387	0.57
0.8	5.6	046	3745	0.87	189	418	0.54
1	5.9	047	5573	0.88	179	449	0.55

3.3. Effect of temperature

The influence of temperature on the inhibition of brass against corrosion was studied by electrochemical techniques already mentioned, with and without the addition of 1 g/L of raw clay for one-hour immersion time in the temperatures between 298K and 328 K. In Fig. 7(a), we note that the temperature has an effect on both branches (cathodic and anodic) and E_{corr} goes to cathodic values by increasing temperature. Besides, the corrosion current density I_{corr} increases and the corresponding inhibition efficiency decreases, probably because of the dissolution of the protective layer [34]. In this part of the study, the potential area was reduced to 300 mV (from -400 mV to -100 mV) to not affect the brass sample at high temperatures.

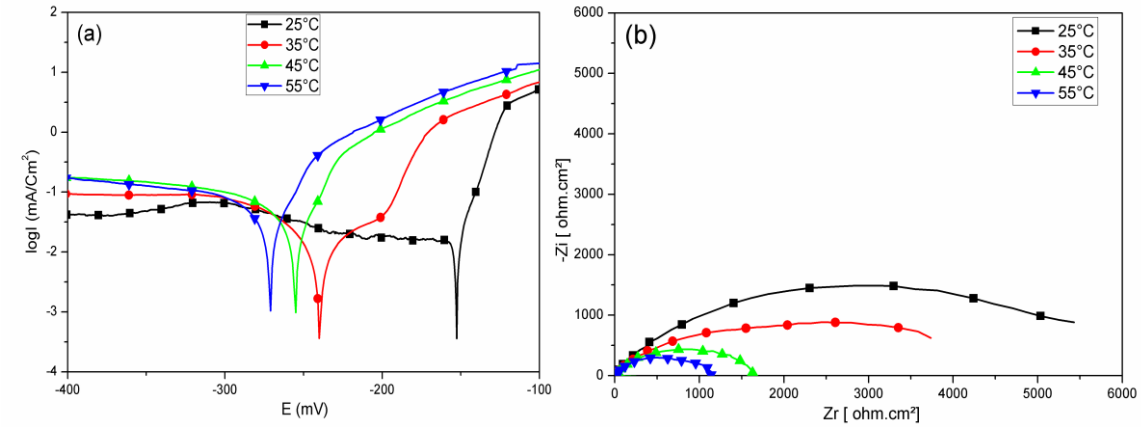

Figure 7. (a) Polarization curves and (b) Nyquist diagrams of brass in presence of 1 g/L of raw Rhassoul at different temperatures.

Nyquist plot in Fig.7 (b) confirms the polarization results by a noticeable decrease in the diameter of the capacitive loop, which leads to a decrease of the inhibition efficiency when increasing temperature. This result has been explained as follows: the interactions between the brass surface

and the protective layer are susceptible to thermal agitation and are easy to break, causing desorption or dissolution when the temperature increases.

3.4. Surface and solution analysis

The surface morphology and composition of the brass samples were investigated by SEM technique and EDS spectra respectively, after polarization tests. Before immersion in the corrosive medium (see Fig. 8 (a) and 8 (a')), the surface appears to be relatively uniform in rough, and little narrow scratches are attributed to the polishing process according to several researchers. This surface is almost recovered by porous layers attributed to hydrozincite $Zn_5 (OH)_6 (CO_3)_2$ and simonkolleite $Zn_5 (OH)_6 Cl_2 - H_2O$ [35,36], and non-porous (Cu-oxide) films of corrosion products (see Fig. 8 (b) and 8 (b')). The addition of 1 g/L of raw clay (see Fig. 8(c) and 8(c')), leads to two areas: a compact precipitated film of Calcite ($CaCO_3$) in neighboring of brass surface explains that the porous film was prevented from growth and a thinner and more compact layer was formed. Yu et al., [17], pointed out the beneficial effect of calcite on corrosion inhibition. The second area is recovered with the clay fraction of Stevensite, leading to a barrier effect on the surface and thus reducing the corrosion products formation.

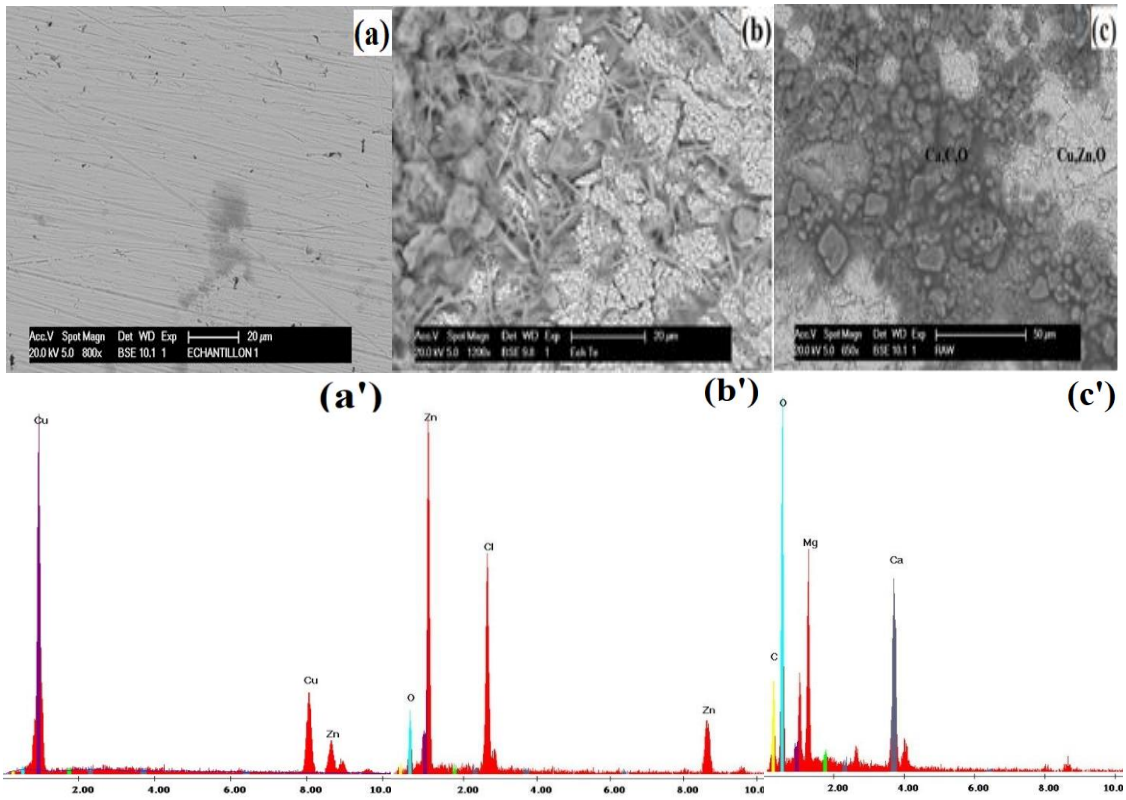

Figure 8. SEM micrographs: (a) before, (b) after immersion in 3% NaCl solution and (c) in the presence of 1 g/L of the raw clay. EDS spectra: (a'), (b') and (c') respectively, of the already mentioned environments.

To determine the amount of Cu and Zn dissolved in the electrolyte, solutions were analyzed by atomic absorption technique after polarization measurements in the absence and presence of the optimum concentration of raw Rhassoul (1 g/L). Table 5 shows the results and indicates that both copper and zinc were present in the electrolyte in small quantities. The Rate release inhibition R_r (%) is calculated using the following equation Eq. 7. Where $C_m(inh)$ and C_m are the concentration of an element in the solution with and without inhibitor, respectively.

$$R_r(\%) = \frac{C_m - C_m(inh)}{C_m} \times 100 \qquad (7)$$

Table 5. Concentrations of Cu^{2+} and Zn^{2+} in the electrolyte in absence and presence of 1 g/L of raw Rhassoul and their release inhibition.

	Cu^{2+} (ppm)	**Zn^{2+} (ppm)**
C_m	11.4	9
C_m(inh)	8.3	3.5
R_r (%)	27%	61%

The release inhibition of Zinc ions Zn^{2+} was higher (61 %) concerning that of Copper ions Cu^{2+} (27 %). This means that the porous layer of Zn-oxide and/or Zn-hydroxide was prevented to forms on the brass surface when adding the optimum concentration of raw clay. This result is in good agreement with that of the surface analysis results.

3.5. Comparative study between raw and homoionic Stevensite Na^+-ST

3.5.1. Electrochemical study

After polarization experiments in 3% NaCl medium, the polarization curves of brass for samples free from clay mineral (Blank) and in the presence of the same concentration of Rhassoul and Na^+-ST (1 g/L) are presented in Fig. 9(a). These curves clearly show both a decrease of the corrosion current density of brass. As we already mentioned, corrosion inhibition is under mixed-type control in the presence of raw Rhassoul. While in the presence of Na^+-ST, current densities of potentials more negative than -500mV disclose the mass transport in the cathodic process. Before the mentioned potential, we observe an activation controlled region (Tafel), where currents were almost linear. In that case, the kinetics of O_2 reduction is governed by its diffusion through the clay mineral layer and the corrosion products film [29]. These results are further confirmed by assessing polarization resistance (R_p) from the impedance modulus at low frequency in the EIS curves. Fig. 9(b) completes the electrochemical study as the diameter of the capacitive loop and the inhibition efficiency decrease when purifying this clay.

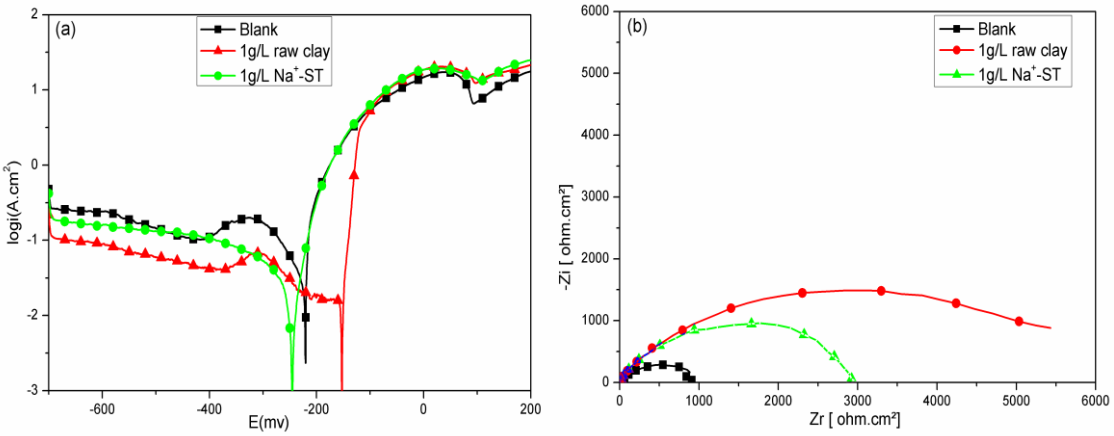

Figure 9. (a) Polarization and (b) Nyquist curves in the presence of the optimum concentrations of raw and Na^+-ST.

As shown in Table 6 indeed, the R_p obtained in the presence of raw clay is 2 times greater than that corresponding to Na^+-ST. Also, this table reports the E_{corr}, and the inhibition efficiency (I_E %) assessed according to the already mentioned relationship Eq. 4. This result can be interpreted by the absence of the main component responsible for the inhibition, which is the calcite layer.

Table 6. Parameters and polarization resistance for brass corrosion in the absence and presence of optimum concentrations of raw Rhassoul and Na^+-ST.

Concentrations	$-E_{corr}$ (mV/SCE)	I_{corr} ($\mu A/cm^2$)	$-\beta_c$(mV/dec)	R_p($\Omega.cm^2$)	I_E(%)
blank	220	73	307	1088	-
1 g/L Rhassoul	151	13.1	161	6030	82
1 g/L Na^+-ST	245	17.4	258	3000	63.7

3.5.2. Surface analysis

To prove the absence of precipitated film of calcite on the brass surface in the presence of Na^+-ST, scanning electron microscope SEM was carried after 1 hour of immersion in 3% NaCl solution after polarization experiments (Fig. 10 (a)). The micrograph shows from one hand, the absence of calcite and presence of some corrosion products, evidenced by the EDS spectrum in (Fig. 10 (b)), leading to a decrease of the inhibition efficiency and from the other hand the surface indicates the presence of the mineral clay components such as: Si, Al, Ca, Mg. Fe... (Fig. 10 (c)) Those elements are attributed to the precipitation of the Stevensite clay fractions. This result lets suggest that this Stevensite layer precipitates on the brass surface, leading to a barrier effect against chloride ions and eventually increases slightly the inhibition efficiency to 63.7 %.

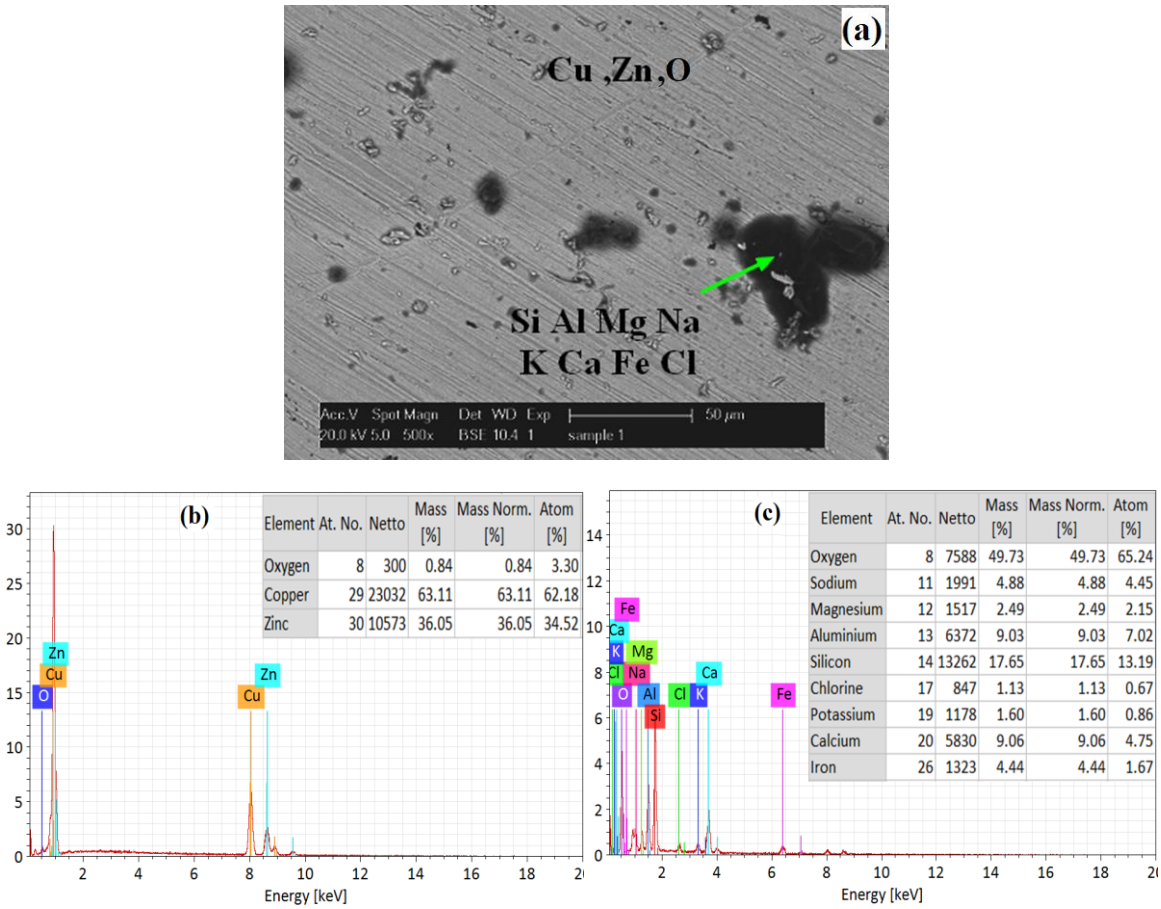

Figure 10. (a) SEM micrograph, (b) and (c) are EDS spectra of the corrosion products and the Stevensite elements respectively, in the presence of 1 g/L of Na^+-ST.

3.6. Effect of pure calcite

3.6.1. Comparison by EIS measurements

To ensure the responsibility of calcite on the inhibition of brass in the previous environment, we chose to compare its inhibition effect with that of Rhassoul and Na^+-ST using the EIS technique. Fig. 11 shows that when using an equivalent concentration of calcite in the electrolyte (0.76 g/L), the shape of the capacitive loop was not modified and that the adjustment to the less chi-square value using EC-Lab program has confirmed the equivalent circuit mentioned in Fig. 5.

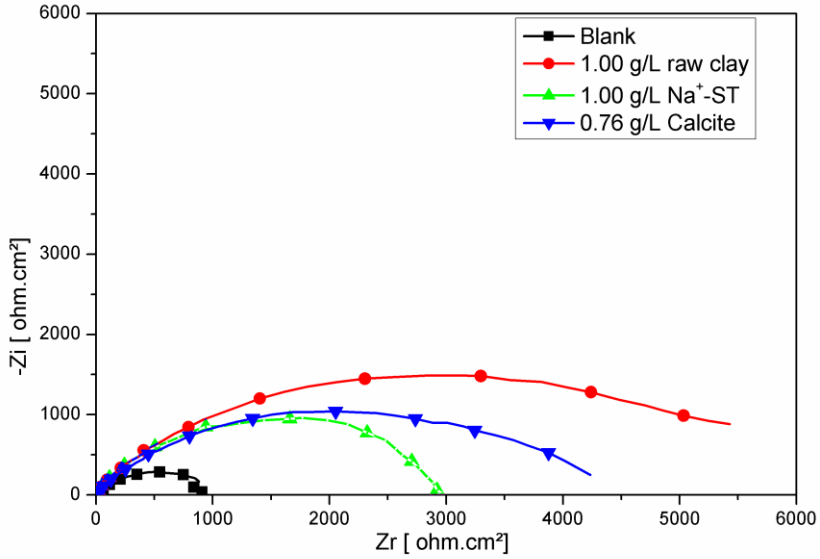

Figure 11. Nyquist plot of brass in 3% NaCl solution in absence and presence of 1 g/L of raw Rhassoul, 1 g/L of Na^+-ST and 0.76 g/L of calcite.

In the presence of calcite, the diameter was one time and a half higher than that obtained with Na^+-ST, but it is equally smaller when using the raw clay. Polarization resistance Rp and the corresponding inhibition percentages E' (%) are shown in Table 7. This confirms that the corrosion inhibition performances exhibited in the presence of raw Rhassoul are better than those observed in the presence of Na^+-ST or pure calcite. Data of this fitting are in good agreement with our interpretations.

Table 7. Rp and E' are values of brass immersed in 3% NaCl medium in the absence and presence of different concentrations of raw Rhassoul.

	Blank	**1 g/L Raw clay**	**1 g/L Na^+-ST**	**0.76 g/L Calcite**
Rp ($\Omega.cm^2$)	1088	6030	3000	4500
E' (%)	-	82.0	63.7	75.8

3.6.2. SEM observation and EDS analysis

In the presence of calcite, the brass surface is covered by a compact layer (Fig. 12(a)). This later is composed of $CaCO_3$, as shown by EDS analysis (Fig. 12(b)). Furthermore, we note the absence of the porous layer attributed to the hydrozincite. Finally, Table 8 shows the number of different elements composing the compact layer, which confirms the precipitation of calcite on the surface.

As evidenced by SEM-EDS and EIS techniques, the synergistic precipitations of calcite and Stevensite clay fraction offer excellent protection against corrosion of brass.

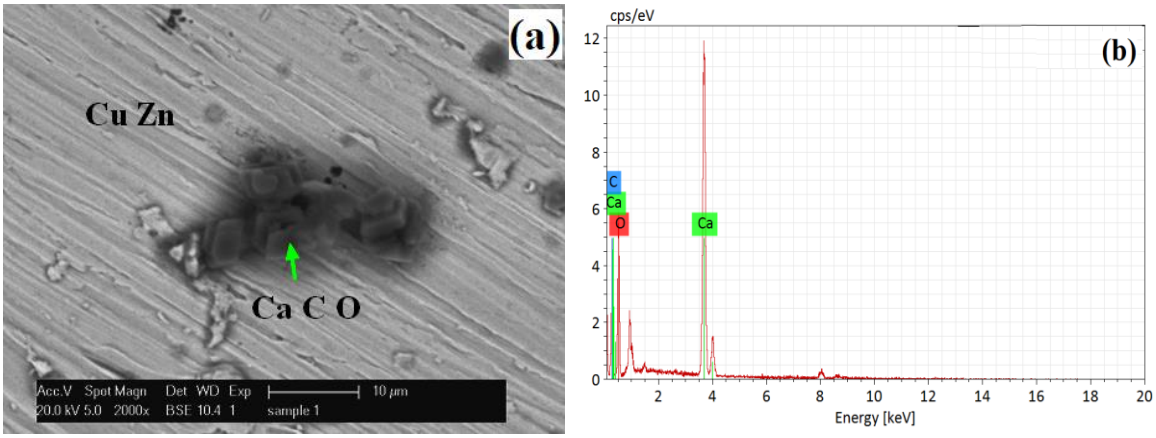

Figure 12. SEM micrograph (a) and EDS spectra (b) of brass surface in the presence of 0.76 g/L of pure calcite in 3% NaCl medium.

Table 8. Composition of different elements composing the brass surface obtained from EDX Analyzer in the presence of 0.76 g/L of pure calcite in 3% NaCl medium.

Elements	**Mass %**	**Atom %**	**Error %**
Carbon	15.44	23.46	0.79
Oxygen	55.50	63.31	2.90
Calcium	29.06	13.23	0.76
Total	100	100	

4. Conclusion

The corrosion behavior of the brass (Cu-36Zn) was investigated by electrochemical measurements in simulated seawater (3% NaCl) in the absence and presence of various concentrations of raw locally Rhassoul and at different temperatures. Thanks to the synergistic effect of calcite and the Stevensite clay fractions presented in this raw clay, this later exhibited a better inhibition efficiency using an optimum concentration of 1 g/L at 298°C. The release of Zinc ions in the electrolyte was inhibited by 61%, measured by atomic absorption technique. SEM-EDS techniques confirmed the precipitation of those components on the brass surface. A spontaneous and relatively strong bond

was occurred with the surface and thus prevents the growth of corrosion products. Separately, Na^+-ST did not show a significant inhibition (63.7%), while pure calcite behaves as main inhibitor presented in this raw clay, reaching 76%. Accordingly, Rhassoul should become a material of choice to protect brass against corrosion in the marine environment.

In order to transfer this research paper to the industrial sector, a new electrochemical study for an appropriate treatment using mineral inhibitor and incorporation of this modified Stevensite X^{y+}-ST into a suitable paint system is carried out.

References

1- M.H. Hussin, M.J. Kassim, The corrosion inhibition and adsorption behavior of *Uncaria gambir* extract on mild steel in 1 M HCl, Mater. Chem. Phys, **2011**, 125, 461-468.
2- F. Mansfeld, T. Smith, E. P. Parry, Benzotriazole as corrosion inhibitor for copper, Corrosion, **1971**, 27, 289- 294.
3- E. Geler, D. S. Azambuja, Corrosion inhibition of copper in chloride solutions by pyrazole, Corros. Sci, **2000**, 42, 631–643.
4- R. Ravichandran, N. Rajendran, Influence of benzotriazole derivatives on the dezincification of 65–35 brass in sodium chloride, Applied Surface Science, **2005**, 239, 182–192.
5- Z. Mountassir, A. Srihari, Electrochemical behaviour of Cu–40Zn in 3% NaCl solution polluted by sulphides: effect of aminotriazole, Corros. Sci, **2007**, 49, 1350–1361.
6- T. Kosec, D. K. Merl, I. Milošev, Impedance and XPS study of benzotriazole films formed on copper, copper–zinc alloys and zinc in chloride solution, Corros. Sci, **2008**, 50, 1987–1997.
7- J. R. Xavier, S. Nanjundan, N. Rajendran, Electrochemical adsorption properties and inhibition of brass corrosion in natural seawater by thiadiazole derivatives: experimental and theoretical investigation, Industrial & Engineering Chemistry Research, **2012**, 51, 30–43.
8- S. Langard, T. Vigander, Occurrence of lung cancer in workers producing chromium pigments, Occupational and Environmental Medicine, **1983**, 40, 71–74.
9- S. A. Katz, H. Salem, The toxicology of chromium with respect to its chemical speciation, J Appl Toxicol, **1993**, 13, 217-224.
10- S. Tazi, I. Raissouni, F. Chaouket, D. Bouchta, A. Dahdouh, R. Elkhamlichi, H. Douhri, The Inhibition effect of Brass corrosion in NaCl 3% by Eugenol, J. Mater. Environ. Sci, **2016**, 7, 1642-1652, https://www.jmaterenvironsci.com/ Document/ vol 7/vol 7_N5/181-JMES-2120-Tazi.pdf.
11- A. Chraka, I. Raissouni, N. Ben Seddik, S. Khayara, A. Ibn Mansour, H. Belcadib, F. Chaouket, D. Bouchta, Aging time effect of Ammi visnaga (L.) lam essential oil on the chemical composition and corrosion inhibition of brass in 3% NaCl medium. Experimental and theoretical studies, Materials Today: Proceedings, https://doi.org/10.1016/j.matpr.**2019**.08.086
12- M. Y. Lvov, G. D. Shchukin, H. Mohwald, R. R. Price, *Halloysite Clay Nanotubes for Controlled Release of Protective Agents*, J. Am. Chem. Soc, **2008**, 2, 814–820.
13- E. Abdullayev, Y. M. Lvov, Halloysite clay nanotubes for controlled release of protective agents, Journal of Nanoscience and Nanotechnology, **2011**, 11, 10007-10026.
14- E. Shchukina, D. Shchukin, D. Grigoriev, Effect of inhibitor-loaded halloysites and mesoporous silica nanocontainers on corrosion protection of powder coatings, Progress in Organic Coatings, **2017**, 102, 60–65.
15- A. Aït Aghzzaf, B. Rhouta, J. Steinmetz, E. Rocca, L. Aranda, A. Khalil, J. Yvon. L. Daoudi, Corrosion inhibitors based on chitosan-heptanoate modified beidellite, Applied Clay Science, **2012**, 65–66, 173–178.
16- A. Aït Aghzzaf, B. Rhouta, E. Rocca, A. Khalil, C. Caillet, R. Hakkou, Heptanoic acid adsorption on grafted palygorskite and its application as controlled-release corrosion inhibitor of steel, Materials Chemistry and Physics, **2014**, 148, 335-342.
17- B.L. Yu, X. L. Pan, J. Y. Uan, Enhancement of corrosion resistance of Mg-9 wt.% Al-1 wt.% Zn alloy by a calcite (CaCO3) conversion hard coating, Corros. Sci, 2010, 52, 1874–1878.
18- A. Aït Aghzzaf, B. Rhouta, E. Rocca, A. Khalil, Grafted palygorskite as containers of heptanoate for corrosion protection of steel in NaCl medium, Corros. Sci, **2017**, 114, 88–95.
19- L. Bouna, B. Rhouta. M. Amjoud, A. Jada, F. Maury, L. Daoudi, F. Senoq, Correlation between electrokinetic mobility and ionic dyes adsorption of Moroccan stevensite, Applied Clay Science, **2010**, 48, 527–530.
20- A. Benhammou, B. Tanouti, L. Nibou, A. Yaacoubi, J. P. Bonnet, Mineralogical and physicochemical investigation of Mg-smectite from Jbel Ghassoul, Morocco, Clays and Clay Minerals, **2009**, 57, 264–270.
21- S. Caillère, S. Henin, M. Rautureau, Minéralogie des Argiles : Classification et Nomenclature, Ed., Masson et INRA, Paris, **1982**.
22- B. Rhouta, H. Kaddami, J. Elbarqy, M. Amjoud, L. Daoudi, F. Maury, F. Senocq, A. Maazouz, J. F. Gerard, Elucidating the crystal-chemistry of Jbel Rhassoul stevensite (Morocco) by advanced analytical techniques, Clay minerals, **2008**, 43, 393–404.
23- T. Holtzapffel, Les mineraux argileux: préparation, analyse diffractométrique et détermination, Ed., Société Géologique du Nord, 1985.
24- A. Benhammou, A. Yaacoubi, L. Nibou,

B. Tanouti, Adsorption of metal ions onto Moroccan stevensite: kinetic and isotherm studies, Journal of Colloid and Interface Science, **2005**, 282, 320–326.

25- L. Bouna, B. Rhouta, M. Amjoud, F. Maury, M. Jada, L. Daoudi, F. Senocq, M. C. Lafont, C. Drouet, Synthèse, caractérisations et tests photocatalytiques d'un matériau argileux d'origine naturelle à base de beidellite fonctionnalisée par TiO2, Matériaux & Techniques, **2012**, 100, 241-252,

26- N. Ben Seddik, I. Raissouni, K. Draoui, A. Aït Aghzzaf, A. Chraka, B. Aznag, F. Chaouket, D. Bouchta,
Anticorrosive performance of lanthanum ions intercalated Stevensite clay on brass in 3% NaCl medium,
*Materials Today: Proceedings, https://doi.org/10.1016/j.matpr.**2019**.08.085*

27- T. Theivasanthi, M. Alagar, physics.chem-ph, Titanium dioxide (tio2) nanoparticles xrd analyses: An insight, **2013**, arXiv:1307.1091.

28- S. Chanel, N. Pébère, An investigation on the corrosion of brass-coated steel cords for tyres by electrochemical techniques, Corros. Sci. **2001**, 43, 413-427.

29- A. Aït Aghzzaf, B. Rhouta, E. Rocca, A. Khalil, J. Steinmetz, Corrosion inhibition of zinc by calcium exchanged beidellite clay mineral: A new smart corrosion inhibitor, Corros. Sci, **2014**, 80, 46–52.

30- E. S. Ferreira, F. C. Giacomelli, A. Spinelli, Evaluation of the inhibitory effect of L-ascorbic acid on the corrosion of mild steel, Mater. Chem. Phys, **2004**, 83, 129–134.

31- I. Aiad, M. M. El-Sukkary, E. A. Soliman, M. Y. El-Awady, S. M. Shaban, Inhibition of mild steel corrosion in acidic medium by some cationic surfactants, J. Ind. Eng. Chem, **2014**, 20, 3524–3535.

32- C. Des louis, B. Tribollet, G. Mengoli, M. Musiani, Electrochemical behaviour of copper in neutral aerated chloride solution. I. Steady-state investigation, J. Applied Electrochem, **1988**, 18, 374–383.

33- Z. Avramovic, M. Antonijevic, Corrosion of cold-deformed brass in acid sulphate solution, Corros. Sci, **2004**, 46, 2793-2802.

34- I. B. Obot, N. O. Obi-Egbedi, Anti-corrosive properties of xanthone on mild steel corrosion in sulphuric acid: Experimental and theoretical investigations, Current Applied Physics, **2011**, 11, 382–392.

35- M. Bitenc, M. Marinsek, Z. C Orel, Preparation and characterization of zinc hydroxide carbonate and porous zinc oxide particles., J. Eur. Ceram. Soc, **2008**, 28, 2915–2921.

36- M. R. Mahmoudian, W. J. Basirun, Y. Alias, M. Ebadi, Synthesis and characterization of polypyrrole/Sn-doped TiO2 nanocomposites (NCs) as a protective pigment, Appl. Surf. Sci, **2011**, 257, 8317-8325.